Optimizing the performance of nickel-like collisionally pumped x-ray lasers. II. Lasers for the wavelength range 50–100 Å

G. J. Pert
Physics Department, University of York, Heslington, York, YO10 5DD, United Kingdom
(Received 19 May 2006; published 7 February 2007)

Soft x-ray lasers operating in the super- 100 Å regime and using grazing incidence pumping methods are now established as efficient sources of radiation in this waveband. The concepts underlying this approach are to separate the ionization and excitation phases of the laser, and to match the pumping density of the latter to the optimal for gain generation. It is therefore of considerable interest to examine whether these ideas can be successfully applied to sub-100 Å lasers. Three problems arise: first the adverse scaling of ionization with temperature for high atomic number ions, second the strong thermal conduction at these temperatures leads to a large hot zone upstream of the absorption, and third the optimum pumping density is greater than the critical density of 1 μm wavelength, solid state pump lasers. Using analytic models and simulation we identify a strategy to overcome these problems using a pre-pulse of a mixed harmonic and fundamental radiation of Nd-glass laser radiation followed by the main pumping pulse of the fundamental normally incident. Due to the large upstream thermal zone and the high ionization temperature, we find that the energy required in the pre-pulse is much (~3 times) larger than that in the main, and that the energy needed consequently scales rapidly with the atomic number and therefore decreasing x-ray wavelength. Systems generating output energies of a few tens of μJ are examined at wavelengths between 50 and 70 Å.

DOI: 10.1103/PhysRevA.75.023808 PACS number(s): 42.55.Vc, 32.30.Rj, 42.60.By, 52.50.Jm

I. INTRODUCTION

X-ray lasers operating in the wavelength region 100 to 200 Å have been greatly improved over the past two years by the introduction of grazing incidence pumping (GRIP) [1–4]. This has improved the efficiency of collisionally pumped nickel-like schemes to such an extent that small scale laboratory application has become practicable. The earlier paper in this series [5] showed that underlying these methods is a clear separation between the initial phase of plasma preparation and the final localised heating at the optimum density. This ensures that the plasma has the correct ionization and a relatively small refractive index variation before the gain is generated. Amplified spontaneous emission (ASE) laser action can then take place efficiently over the entire length of the plasma body. The plasma is generated as a large aspect ratio cylinder so that amplification takes place preferentially along the axis.

There has long been considerable interest in trying to drive these lasers to shorter wavelengths. In the early days of plasma x-ray lasers, ions such as nickel-like gold and tantalum were successfully, albeit weakly, pumped to lase on a number of transitions between 36 and 72 Å [6–9], but these were only accomplished by using very large energies from the NOVA laser. Since then there have been relatively few observations of sub- 100 Å lasers using more efficient techniques. The shortest wavelength achieved, dysprosium, at 59 Å, was driven into saturation [10] using a double pulse of 75 ps duration. Following the introduction of CPA (chirped pulse amplification), short pulses were very successfully used to heat a prepared plasma. However, only two sub-100 Å experiments have been carried out one with lanthanum at 88 Å [11] and one with samarium lasing at 72 Å [12]. Shorter wavelengths have been attempted but failed as the laser energy was insufficient.

In our recent paper [5], we explored the underlying physics of CPA pumped systems in the super-100 Å wavelength range. It was concluded that some improvements in the pumping of samarium could be effected, but that these methods would start to fail at shorter wavelengths. In this paper we use the general principles enunciated in that work to try to develop sub-70 Å lasers with a minimum of input energy. It is found that the underlying physics is changed from that for elements lasing at above 100 Å, and that different constraints are placed on the design.

II. METHODOLOGY

In this paper we shall initially explore the basic physics of the laser interaction with the target necessary to generate plasma with the required ionization. This will be based on simple approximate, well established analytic models of laser plasma generation, together with approximate steady state models of the ionization and atomic physics. The scalings so derived will give a clear identification of the key difficulties in driving plasma based lasers to short wavelengths.

These scalings will underpin the results obtained by direct simulation discussed in this paper, using the simulation model EHYBRID (Appendix A), and x-ray beam production with RAYTRACE (Appendix B). EHYBRID is used to calculate the development of the plasma from solid slab targets, and the spatial development of the spontaneous emission rates, gain and refractive index within the plasma body. This data is then used as input to the ray tracing code (RAYTRACE) to generate the resultant power distribution as functions of the spatial and angular co-ordinates at the exit of the laser. Since each output is calculated at a single instant in time, the calculation must be repeated many times and the output integrated to obtain the total energy output from the laser. It is

implicit in the form of this calculation that the laser is travelling wave matched, so that the pump laser pulse and the x-ray output travel synchronously along the laser axis.

The present study will be limited to cases in which the width of the focal spot is sufficiently large that the plasma development is essentially one dimensional. This allows us to use simple laser ablation models to describe the plasma formation, which can be compared with the simulation outputs. Although helpful these will be found to have their limitations, but will however, help in elucidating the essential features of these concepts.

In assigning the starting condition to EHYBRID it is necessary to specify the initial plasma width. This has been normally taken to be the full width half maximum (FWHM) of the Gaussian focal spot, so that the plasma does not fully fill the laser beam. Two dimensional simulations, not discussed here, have shown that this is a reasonable approximation. Thus the nominal input energies used must be reduced by a fill factor of approximately 0.8 to obtain the energy incident on the plasma. In all the simulations presented here the focal spot FWHM is taken to be 100 μm.

The pulses are assumed to be generated by a Nd-glass laser, so that the fundamental wavelength is 1.06 μm and the harmonic 0.53 μm. The temporal shape of the pulses may take one of two forms: a trapezoidal pulse or a modified Gaussian pulse. For each pulse we specify the rise and FHWM times. In this work the pre-pulse is taken as a trapezoidal pulse of 10 ps rise time and specified FWHM half-width, the main pulse as a Gaussian of 1 ps rise time and 2 ps FWHM half-width. The onset of the main pulse is taken to be at the termination of the pre-pulse. This avoids the losses due to thermal conduction and recombination, which would otherwise degrade the plasma generated by the first pulse. Times are measured throughout from the onset of the second (main) pulse.

Absorption is principally by inverse bremsstrahlung. For light incident at non-normal angles resonance absorption determined by the analytic expression at low intensity is used. However, at normal incidence a dump at the critical density is set by a reflectivity, R. In the case where inverse bremsstrahlung absorption is weak, the modelling is strongly dependent on the poorly known value of this quantity, R. The value used in this work, $R=0.7$, is based on the considerable body of experimental data obtained several years ago. It was found in a series of experiments carried out in different laboratories that as the irradiance increased, and before the onset of nonlinear effects, the absorption "saturated" at a "universal" value of about 30% (see for example the summary by Ahlstrom [13]). This was interpreted as absorption at the critical density as inverse bremsstrahlung in the bulk plasma became weak due to the high temperature. The absorption was supposed to be due to resonance absorption in surface ripples and to enhanced inverse bremsstrahlung due to the refractive index "swelling" near critical. Fortunately the systems we investigate here are relatively insensitive to this parameter.

The second rather arbitrary parameter we include is the flux limiting factor, f. This term is used to give a local modification to the thermal conduction heat flux to take account of large temperature gradients. Although a nonlocal phenomenon, it is normal to use a local description modifying the thermal conductivity, provided the effect is not strong. A flux limiting factor $f=0.1$ has been used in this work, which is consistent with more complete modelling.

In earlier work we introduced an empirical laser flux reduction, F, whose values ranged from 0.5 [14] to 0.3 [12] to fit to experiments. In more recent work modelling the experiments of Dunn [15] using palladium and silver we have not found it necessary to introduce this factor. Although no unequivocal explanation of the origin of the term has yet been found, we believe it was associated with beam and focusing imperfections, and nonlinear reflection in those experiments. One factor contributing to this term is the fill of the finite plasma width by the assumed Gaussian focal profile. In these simulations, the fill factor was typically 0.78. The values of irradiance and energy given in this work have not been modified by this factor, i.e., F is set to unity, although the fill factor is explicitly used to derive the incident irradiance.

A number of simulations have been ray traced to examine the effects of refraction, saturation, and other effects, and to calculate estimates of the output power and energy. In all these calculations the plasma length has been taken to be 1 cm.

III. ANALYTIC APPROXIMATIONS

One dimensional plasma generation by laser irradiation is described by a simple hydrodynamic model closely resembling the classical Chapman-Jouget deflagration [16,17] in which the heat release is provided by laser absorption instead of chemical reaction. Heat dispersal stabilizes the flow by self-regulating mechanisms, and is provided by either thermal conduction or by inverse bremsstrahlung absorption or by a combination of the two. Two simple analytic approximations exist, which are limiting solutions of a more general case, somewhat misleading named the "deflagration" and "self-regulating" models.

A. Deflagration model

At high irradiance the plasma is too hot to absorb strongly by inverse bremsstrahlung, so that radiation penetrates to the critical density, n_c, where it is either reflected or strongly absorbed by a number of possible mechanisms including enhanced inverse bremsstrahlung (due to the refractive index swelling factor), resonant absorption or nonlinear-parametric processes. The absorption is therefore localized at the critical density and the heat distributed by thermal conduction [18–20]. The downstream flow is assumed to be an isothermal rarefaction, and the critical density layer the isothermal thermal sonic point. This model scales the electron temperature as follows:

$$T_e \approx 0.397 \frac{1}{\alpha \bar{Z} R_g} \rho_c^{-2/3} \Phi'^{2/3}, \tag{1}$$

where Φ' is the net absorbed energy flux balanced against the thermal and kinetic fluxes, and $\rho_c = M n_c / \bar{Z}$ the mass density, $\bar{Z}$ ($=Z-28$ for Ni-like ions) the ionization, $\alpha=1.0$

$+T_i/(\bar{Z}T_e)$ and $R_g=k/M$ the gas constant per unit mass; T_i being the ion temperature and M the atomic mass. The flux Φ' therefore neglects ionization and any other energy losses associated with radiation for example. The mass flux is constant with value

$$\dot{\mu} \approx 0.630\rho_c^{2/3}\Phi'^{1/3}. \tag{2}$$

B. Self-regulating model

At low irradiance the plasma is relatively cold, and, due to their temperature dependences, thermal conduction relatively weak, but inverse bremsstrahlung strong [21,22]. In consequence the heat release is distributed over the entire plasma bulk, but concentrated in a region near the isothermal sonic point. In contrast to the previous case the flow is unsteady as the plasma growth changes the optical depth, and consequently the heat deposition profile. Using cgs units, the pattern may however, be described by a self-similar form in which the temperature at the isothermal sonic point scales as follows:

$$T_e \approx 0.423\frac{1}{\alpha\bar{Z}R_g}b^{1/4}\Phi'^{1/2}\tau^{1/4}, \tag{3}$$

where τ is the pulse duration, $b=5.492\times10^{36}(\alpha^{3/2}\bar{Z}^{9/2}/A^{7/2})\lambda^2\ln\Lambda_a$, $\ln\Lambda_a=\ln(3.07\times10^5\bar{Z}^{-1}\lambda T_e^{3/2})$ being the Coulomb logarithm for absorption. The mass ablation rate

$$\dot{\mu} \approx 0.559b^{-1/4}\Phi'^{1/2}\tau^{-1/4} \tag{4}$$

and the sonic point density

$$\rho_a \approx 0.784b^{-3/8}\Phi'^{1/4}\tau^{-3/8}. \tag{5}$$

The numerical values are taken from the approximate solution given in Ref. [23], which is based on a direct analogy with the deflagration model. The close relationship between these two models can be seen by eliminating $b\tau$ from Eqs. (3) and (4) using (5) and comparing with Eqs. (1) and (2). We note that the difference between this set of values and those generated by exact calculation is small.

The self-regulating model is appropriate when the absorption density, ρ_a, is small compared to the critical density.

C. Thermal conduction zone

In the deflagration model the absorption is localized at a specific "absorption surface" [19]. In the self-regulating model on the other hand the absorption is distributed. However, in the latter case, we may, with only small error, separate the flow into two regions at the sonic surface where the flow speed equals the isothermal sound speed [23]. The downstream flow can be represented by an isothermal rarefaction heated by absorbed laser radiation, and the upstream by a quasisteady flow in which further absorption is taking place. In planar geometry, the general case involving both thermal conduction and inverse bremsstrahlung absorption is not amenable to simple analysis. However, when the temperature is high, this upstream region is narrow, and we may again consider a fraction of the energy to be absorbed at this "front," but whose density is determined by collisional absorption rather than the critical density [24]. An approximate result is obtained by taking the absorption density to be the sonic density from Eq. (5).

Between the absorption region and the undisturbed material there will be a region heated by upstream thermal conduction bounded by a sharp heat front. The form of this layer when flux limitation is taken into account was given by the author [20]. It was shown that the thickness of the layer is determined by the upstream thermal conduction scale length, $L=6T_e/\nabla T_e|_a$ at the absorption surface. The length, mass, and total thermal and kinetic energy of this region are, respectively,

$$\beta_l L; \quad \beta_m\rho_a L; \quad \beta_e\rho_a EL, \tag{6}$$

where $E=c^2=p/\rho=\alpha\bar{Z}kT_e/M$ is the square of the isothermal sound speed at the absorption surface. The constants β are obtained by integration over the heat front profile. For a flux limiter of $f=0.1$ in the materials of interest these take the values $\beta_\ell\approx0.0629$, $\beta_m\approx0.1767$, and $\beta_e\approx0.1580$. The length L can be written in the form

$$L=\frac{\kappa_a T_{ea}}{\frac{1}{2}\rho_a c^3}=\frac{2aE^2}{\rho_a}, \tag{7}$$

where $a\approx1.5\times10^{-32}[A/(\alpha\bar{Z})]^{7/2}/(\bar{Z}\ln\Lambda_T)$ in cgs units, and $\ln\Lambda_T$ is the Coulomb logarithm for transport [25]. The total energy in this region will also include the ionization, neglected above. We note that if the slow variation of the ionization temperature and the Coulomb logarithm are neglected, the mass and energy parameters are both independent of the absorption density.

In the self-regulating regime, we may determine whether the thermal conduction zone is "thick" or "thin" by comparing the penetration upstream of the sonic point with that of thermal conduction, whose ratio is

$$6.301a^{-1}b^{-3/4}\Phi'^{-1/2}\tau^{1/4}. \tag{8}$$

At high power when Φ' is large, this ratio is small and thermal conduction dominates, and *vice versa*.

In the more general case where absorption occurs both close to the critical density and within the plasma plume, and thermal conduction is active, we may expect that the actual values will lie between the two limits. The transition from one model to the other occurring when $\rho_a\sim\rho_c$.

IV. IONIZATION

In order to achieve wavelengths less than about 80 Å it is necessary to use ions of atoms of relatively high atomic number ($Z\gtrsim60$). Under these conditions recombination and thermal conduction play a important role in determining the plasma state. Since ionization is a relatively slow process, it is advisable to prepare the plasma to near the required Ni-like ionization condition before the main pulse is applied, rather than allowing further ionization in the main pulse

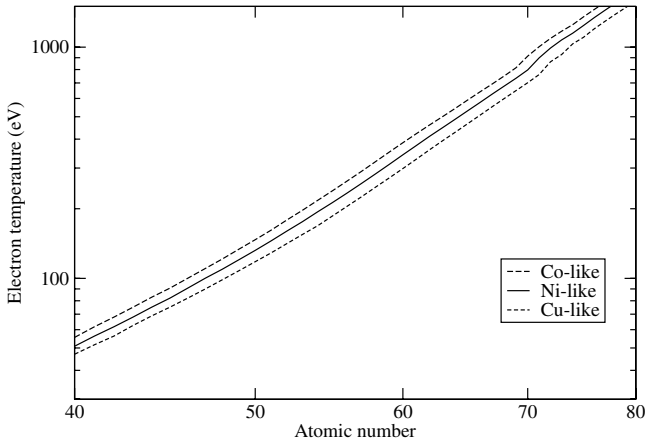

FIG. 1. Plot of the steady state electron temperature necessary to achieve ionization to the copper, nickel, and cobaltlike stages as a function of the atomic number Z at electron density 10^{21} cm^{-3}

heated plasma. This places a necessary constraint on the prepulse, which must prepare both the ionization and the density profile at suitable values.

Figure 1 shows the electron temperature, T_e, required to achieve the copper, nickel, and cobaltlike ionization stages in the steady state as a function of the atomic number Z at an electron density of 10^{21} cm^{-3}. This is calculated by balancing the upward (excitation/ionization) processes against the downward (de-excitation/recombination) to give the population ratio for each ionization stage, and hence since the total ion population is unity, the actual ionization $\bar{Z}$. The lowest ionization stages are treated by the simple modified Griem's model, but all stages higher than the calcium-like are calculated using a set of 4 screened hydrogenic states and the collisional-radiative model [26]. We find that for $Z \gtrsim 55$ the dependence of T_e on Z can be represented as a power law, as can be clearly seen in Fig. 1. For Cu, Ni, and Co-like ionization stages in the range of $55 < Z < 80$ and electron density $5 \times 10^{20} < n_e < 10^{22}$ cm^{-3} we find empirically that the electron temperature scales for the different ionization stages scale in a approximately similar fashion with atomic number

$$T_e \approx A_{ion} Z^{5.5}, \tag{9}$$

where the constant A_{ion} takes the values given in Table I when the temperature is in eV. The departure from this scaling for small Z is due to the relative importance of three body recombination at these colder temperatures and relatively high density. This departure from the scaling of Eq. (9)

TABLE I. Ionization temperature scaling parameters A_{ion} (eV) from Eq. (9).

Density (cm^{-3})	Cu-like	Ni-like	Co-like
5×10^{20}	5.46×10^{-8}	6.18×10^{-8}	6.82×10^{-8}
10^{21}	5.2×10^{-8}	5.87×10^{-8}	6.48×10^{-8}
4×10^{21}	4.6×10^{-8}	5.07×10^{-8}	5.46×10^{-8}
10^{22}	4.26×10^{-8}	4.69×10^{-8}	5.12×10^{-8}

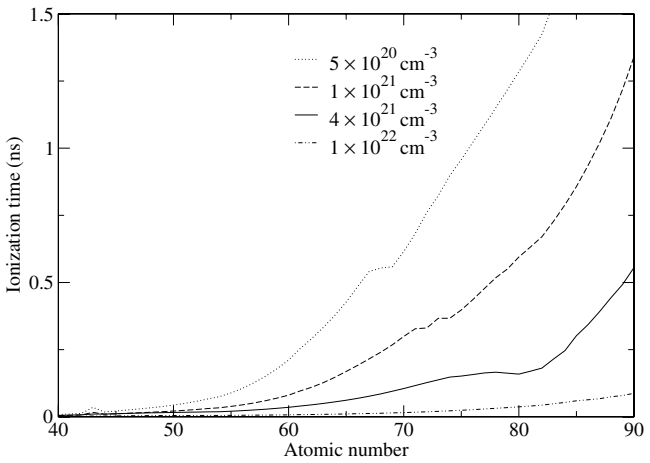

FIG. 2. Plot of the time taken to reach the Cu-like ion stage for plasma at the steady state electron temperature necessary to achieve ionization to the Ni-like stages as a function of the atomic number Z at electron densities 10^{21} and 4×10^{21} cm^{-3}.

moves to higher atomic number as the density is increased, from $Z \approx 45$ at $n_e \approx 5 \times 10^{20}$ cm^{-3} to $Z \approx 55$ at $n_e \approx 4 \times 10^{21}$ cm^{-3}.

V. IONIZATION TIME

Ionization is a relatively slow process, whose duration will determine the necessary pulse duration of the ionizing pulse. Since the time taken to reach the equilibrium state described in the previous section is effectively infinite, we must be prepared to work at a slightly higher temperature before complete ionization is achieved. We have therefore calculated the time taken for ionization to reach the stage 1 below the equilibrium value in a plasma at the equilibrium temperature; for example to reach the Cu-like stage at the Ni-like ionization temperature. The results at densities of 5×10^{20} to 10^{22} cm^{-3} are shown in Fig. 2. We can see that the time scales roughly inversely with density as expected. More importantly we note that the times are long at the lower density ($\sim$1 ns) and rapidly increase for $Z > 80$. At the higher density, for $Z \lesssim 75$ the times are about 200 ps, which is consistent with pumping at the harmonic of the Nd glass laser.

Ionization is a slow process, and it may be necessary to heat the plasma to higher temperature to achieve the required ionization during the pre-pulse. Nonetheless the temperatures given by Eq. (9) are a lower bound to those needed, and therefore useful to develop the scaling. We will find that except at the largest atomic numbers considered here, they give a reasonably accurate estimate of the temperatures required.

VI. OPTIMUM PUMPING DENSITY

We showed, in our earlier work [5] that there is an optimum density for maximising the fractional population inversion (F_{PI}), defined in Eq. (10) in these systems. In consequence there is also an electron density at which the gain is

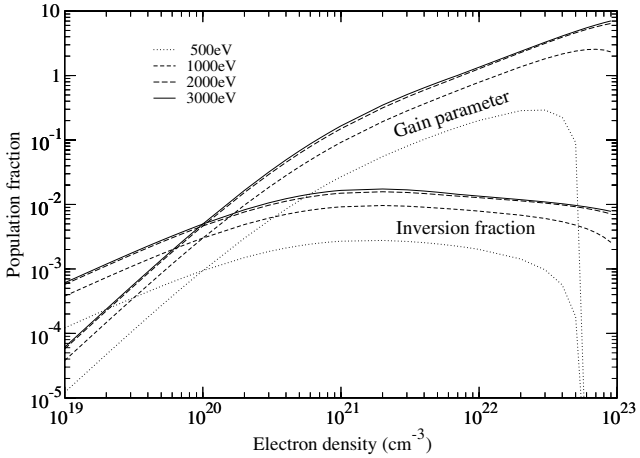

FIG. 3. Plots of the inversion fraction and gain parameter for dysprosium for a range of temperatures.

maximized, although the two values will be different due to the direct linear dependence of the gain on density. As the atomic number gets larger the optimum density increases. Figure 3 illustrates this fact for dysprosium (Z=66). The plot shows essentially the same terms as in [5], namely the inversion fraction (F_{PI}) and gain parameter (G) but calculated as fractions of the ground state population of the Ni-like ion.

$$F_{\mathrm{pi}} = \frac{1}{q_0}\left\{\frac{q_2}{g_2} - \frac{q_1}{g_1}\right\},$$

$$G = 10^{-20} n_e \times F_{\mathrm{pi}}, \tag{10}$$

where q_0, q_1, q_2 and g_0, g_1, g_2 are the populations and statistical weights of the ground, lower and upper laser states, respectively, and n_e the electron density. The gain parameter is the product of the inversion fraction and the electron density. However, some care must be exercised in interpreting this graph, as it must be remembered that the actual gain will depend on the product of the gain parameter and the ground state density, which will be determined by the ionization discussed in the previous section. In contrast to silver and samarium it can be seen that we have not reached the maximum on the gain curve at electron density 10^{22} cm^{-3}, but that the inversion fraction is reasonably constant above 10^{21} cm^{-3}.

We note that in the range of 1–3 keV, the inversion depends only weakly on the temperature. However, these temperatures are significantly higher than the ionization temperature, namely 572 eV. Although the inversion is weaker at this temperature it is nonetheless significant at this lower temperature provided the electron density is less than about 5×10^{22} cm^{-3}, where the characteristic high density fall off occurs. As a result we may expect that weak gain will be established by the conclusion of the ionization phase—a result confirmed in our simulations. This is the origin of the relatively strong gain seen in the early single long pulse foil experiments [6].

VII. MODEL IRRADIANCE

We may use the preceding deflagration and self-regulating plasma generation models [Eqs. (1) and (3), respectively] together with the ionization temperature data (Fig. 1) to calculate the necessary irradiance to produce the required ionization stage. However, we note that the irradiance used in the preceding equations is incomplete as it does not include the energy required for ionization which must also be supplied from the laser beam. Since the total mass of ablated plasma, given by Eqs. (2) and (4), respectively, is assumed to be ionized, the total irradiance required is:

$$\Phi = \Phi' + V_{ion}\tau^{-1}\int_0^\tau \dot{\mu} dt, \tag{11}$$

where V_{ion} is the total ionization energy of all stages up to the one required. In making this estimate we have neglected the ionization of the upstream plasma heated by thermal conduction. At the termination of the pulse this may contain a significant amount of energy due to both the temperature and ionization, although the latter is probably not complete.

Figure 4 shows the rapid increase in the irradiance from a laser of pulse length 100 ps at the harmonic wavelength

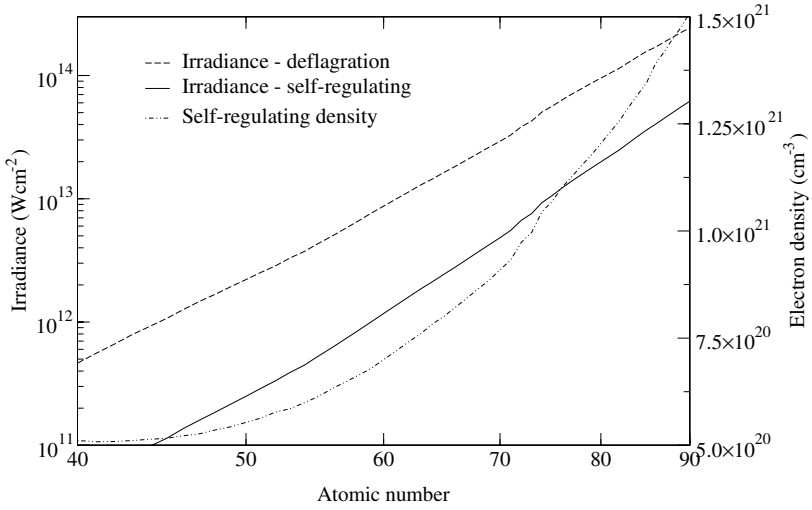

FIG. 4. Plot of the irradiance (including the ionization energy) required from lasers of duration 200 ps and wavelength 0.5 μm to reach the Cu-like ionization stage as a function of the atomic number Z using the deflagration and self-regulating models. The irradiance, Eq. (11), neglects upstream thermal conduction. The ablation density from the self-regulating model is plotted to show that it is significantly less than the critical under these conditions.

TABLE II. Irradiance scaling parameters A from Eq. (12).

		A_{sr}(W cm^{-2})	
Wavelength (μm)	A_d(W cm^{-2})	100 ps	200 ps
1.06	4.7×10^{-3}	1.3×10^{-6}	9.5×10^{-7}
0.53	1.8×10^{-2}	2.6×10^{-6}	1.8×10^{-6}

0.5 μm required to attain the Cu-like ionization stage [$\bar{Z}\approx(Z-29)$] as the atomic number Z is increased when $\alpha\approx1$. This plot is representative of others at different wavelengths and pulse durations in that again there are simple scalings for the irradiance as a function of the atomic number valid for $Z\gtrsim55$ similar to Eq. (9). The deflagration and self-regulating flows both follow these forms with different powers, namely

$$\Phi=\begin{cases}A_dZ^{8.25} & \text{Deflagration},\\ A_{sr}Z^{10} & \text{Self-regulating}.\end{cases} \tag{12}$$

If we adopt the ionization/temperature scaling of Eq. (9) and assume $\bar{Z}\sim Z$, we find the scalings for the irradiance neglecting ionization as $\Phi'\sim Z^{33/4}$ for the deflagration and since $\bar{Z}/A\sim Z^{0.5}$, $\Phi'\sim Z^{10}$ for the self-regulating model in good agreement with the above expressions. The thermal exit flux dominates the ionization for $Z\gtrsim60$ as noted earlier, which is in accord with the departure of the observed plots from the scalings below this value. The values of the constants A_d and A_{sr} in W cm^{-2} are given in Table II, noting that the irradiance required by the deflagration is independent of the pulse length.

We can observe the scaling of the irradiance with pulse length and wavelength from Table II. We see that in the deflagration regime the doubling the wavelength leads to an increase in the irradiance by a factor 4, in conformity with Eq. (1), which predicts that the input power density varies with wavelength as $\Phi\sim\lambda^{-2}$. In the self-regulating mode the changes, of factors 2 are consistent with $\Phi\sim\lambda^{-1}$, given by the model, Eq. (3). The temporal scaling of the deflagration is constant as expected, whereas the self-regulating model, showing a common decrease of about a factor of 1.35 for a doubling of the pulse length, is also consistent with the predicted scaling $\Phi\sim\tau^{-1/2}$, Eq. (3).

To identify which limit is appropriate, we estimate the electron density at the isothermal sonic point for both the fundamental and harmonic wavelengths. These results show an simple empirical scaling relation for $Z\gtrsim60$ in good agreement with Eq. (5)

$$n_{e_{sr}}\approx1.32\times10^{18}\tau(\text{ps}^{-1/2})\lambda(\mu\text{m}^{-1})Z^2\text{cm}^{-3}. \tag{13}$$

Since the critical density at 0.53 μm is 4×10^{21} cm^{-3}, it is evident that the entire flow is consistent with inverse bremsstrahlung heating over the range of pulse lengths considered here. However at 1.06 μm the flow is transitional for high atomic numbers and long pulses. The use of shorter wavelength harmonic radiation will therefore maintain the distributed inverse bremsstrahlung absorption to higher atomic numbers.

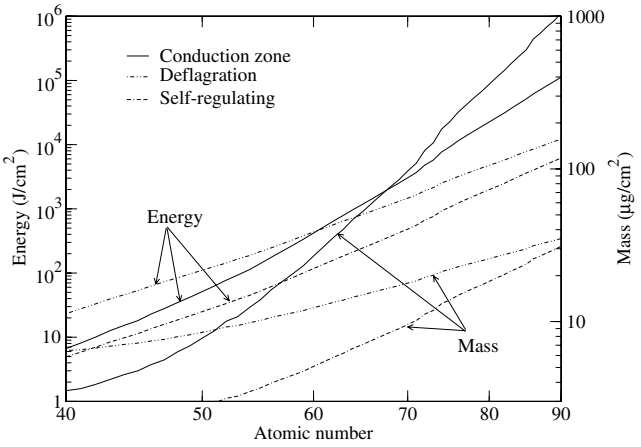

FIG. 5. Comparison of the mass and energy stored in the ablation zone with that in the corona at the ionization temperature of an electron density of 10^{21} cm^{-3} for Cu-like ions and a pulse length of 200 ps.

These values are still incomplete in that we have not included the heated mass upstream of the absorption surface, which is both hot and ionized. As an estimate of the energy located in this region at the end of the pulse we calculate the total thermal and ionization energy assuming the entire mass is ionized to the copperlike stage. The mass and energy in this region when thermal conduction dominates are given by Eq. (6) and the data in Fig. 1. Equations (6) and (9) together with the approximate scalings $\bar{Z}/A\sim Z^{1/2}$ and $\bar{Z}\sim Z$, which are reasonably accurate for $Z>60$, give scalings for mass $M\sim Z^{37/4}$ and energy $E\sim Z^{61/4}$. In fact it can be shown that good fits to the mass and energy data calculated in this manner are given by

$$M\approx2.55\times10^{-15}\,Z^9\ \mu\text{g/cm}^2,$$

$$E\approx6.83\times10^{-22}\,Z^{13.4}\ \text{J/cm}^2, \tag{14}$$

valid for $Z>60$. Since the mass and energy are not directly dependent on the absorption density, the only density variation occurs through the temperature in Eq. (9). At large atomic numbers we observe the rapid growth of both the total energy and mass of this layer. Indeed the plasma mass and the energy lost by thermal conduction exceed the total outflow into the plasma corona given in Fig. 4 for values of $Z\gtrsim60$ in the deflagration picture and all values of Z in the self-regulating. This is illustrated in Fig. 5 for pulses of duration 200 ps.

VIII. COMPARISON WITH SIMULATION

As a useful comparison we may compare the values generated by the models with the irradiance used in the simulations reported both in our earlier paper [5] and in the work reported here. Since the analytic models assume a uniform focal spot and complete absorption, we must correct the simulation values for the incompletely filled Gaussian focal spot using the calculated fill factor, and for incomplete absorption due to the reflectivity (0.7) at the critical surface. In

TABLE III. Comparison of the analytic model with simulation values for the irradiance needed to generate Cu-like ionization.

Element	Wavelength	Pulse length	Self-reg Density	Self-reg Irradiance	Deflagration Irradiance	Burn Irradiance	Total Irradiance	Simulation Irradiance
Z	μm	ps	cm^{-3}	W cm^{-2}	W cm^{-2}	W cm^{-2}	W cm^{-2}	W cm^{-2}
47	1.06	600	1.5×10^{20}	4.6×10^{10}	3.6×10^{11}	4.7×10^{10}	9.3×10^{10}	8.3×10^{10}
62	1.06	290	3.0×10^{20}	6.6×10^{11}	2.8×10^{12}	2.2×10^{12}	2.9×10^{12}	2.4×10^{12}
64	1.06	290	3.2×10^{20}	8.8×10^{11}	3.6×10^{12}	3.3×10^{12}	4.2×10^{12}	4.3×10^{12}
64	0.53	290	6.5×10^{20}	1.8×10^{12}	1.4×10^{13}	3.3×10^{12}	5.1×10^{12}	4.3×10^{12}
66	0.53	100	1.2×10^{21}	4.0×10^{12}	1.8×10^{13}	1.4×10^{13}	1.8×10^{13}	1.8×10^{13}
66	0.53	200	8.2×10^{20}	2.8×10^{12}	1.8×10^{13}	7.0×10^{12}	1.0×10^{13}	1.2×10^{13}
70	0.53	100	8.2×10^{20}	6.8×10^{12}	2.9×10^{13}	3.0×10^{13}	3.7×10^{13}	3.5×10^{13}
70	0.53	200	9.1×10^{20}	4.8×10^{12}	2.9×10^{13}	1.5×10^{13}	2.0×10^{13}	3.1×10^{13}
70	0.53	300	7.4×10^{20}	3.9×10^{12}	2.9×10^{13}	1.0×10^{13}	1.4×10^{13}	2.2×10^{13}
70	0.53	400	6.4×10^{20}	3.4×10^{12}	2.9×10^{13}	7.5×10^{12}	1.1×10^{12}	1.6×10^{13}

our earlier work, the pre-pulse plasmas are all formed by normally incident light at the fundamental wavelength. Table III compares the values obtained from Eqs. (1) and (3), and the equivalent irradiance determined by the energy held in the burn divided by the pulse duration. The total flux is the sum of the self-regulating flux and the equivalent thermal conduction flux, which should be compared with the adjusted values from simulation. The results very clearly show behavior in the self-regulating flow picture regime. However, for all larger atomic numbers (excluding silver, $Z=47$), the strong thermal conduction into the solid dominates the energy flux into outflow. With the exception of ytterbium ($Z=70$), there is acceptable agreement between our models and the simulation. We note however, that the models in their simple form tend to slightly overestimate the values from a more complete calculation. This can be accounted for by the assumption of a uniform degree of ionization throughout the plasma assumed in the model.

The values for ytterbium are taken from simulations using a mixed harmonic+fundamental beam, and assume for reasons noted later, that the two plasmas are broadly similar. However, ytterbium represents a special case as the ionization time is longer than the pulse durations considered in these simulations so that the ionization does not reach a steady state within the time. We will examine this case latter.

IX. PRE-PULSE IONIZATION

We are now in a position to try to use the preceding results to identify the conditions required by the pre-pulse to get the necessary ionization. We recall that the pre-pulse should satisfy three conditions: (i) Generate ionization at least to the Cu-like ion stage; (ii) Produce a relatively slowly decreasing density in the corona; (iii) Operate with as low energy as possible.

We have identified the Cu-like stage as the lowest necessary for generating inversion on the Ni-like ion. The reason for this is twofold. First when the ionization is Cu-like there is a significant population of Ni-like ions, which can be inverted. Second further ionization of these stages at these temperatures is slow, and use of the main pulse for further ionization is wasteful due to the losses during ionization. The long times needed to reach the Cu-like ionization at the equilibrium temperature for Ni-like ions imply the use of long pulses at high power. It is more efficient to use higher power but for a shorter time.

To address the second point we can use the results from Eqs. (2), (4), and (5) to show that the scale size of the dysprosium plasma from the deflagration model at 200 ps is about 21 μm and from the self-regulating 25 μm. Since refraction is less severe at these shorter wavelengths we may conclude that this is a sufficiently long pulse duration, a result which will be confirmed by simulation. The choice of wavelength is governed by the optimal density for pumping. Two criteria govern this choice. First the shorter ionization times at higher density (Fig. 2) and second the higher operating density (Fig. 3). Since the critical density for harmonic Nd-glass radiation is 4×10^{21} cm^{-3} there is clear merit in using this wavelength. In view of the efficiency of thermal conduction at these densities, we may however, improve our overall input efficiency by using the unconverted fraction of radiation as an additional pump. Again simulation will confirm the effectiveness of this conclusion.

The effect of changing the wavelength of the irradiating light is shown by comparing the two sets of results shown in Table II. Thus if the wavelength of the beam is shortened to 0.5 μm the required irradiance is increased for each model. However, commensurate with the change introduced by the scaling of each model is the switch back from a deflagration type flow toward a self-regulating due to the increase in the critical density. The consequence is that the total input flux required is nearly the same for both wavelengths. We note also that for atomic numbers in our range of interest, $Z\approx60-70$ the sonic density from the self-regulating model is approximately our working density $n_e\approx10^{21}$ cm^{-3}.

We will now examine these issues in more detail by the use of specific examples with gadolinium and dysprosium as typical cases.

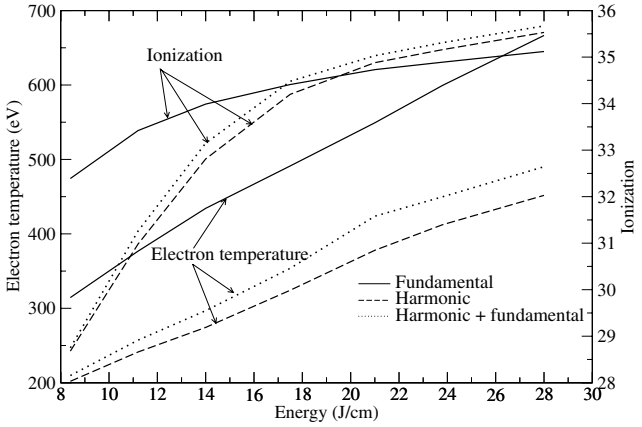

FIG. 6. Plots of ionization and electron temperature in gadolinium heated by a pre-pulse of 290 ps duration as function of the laser energy for different wavelengths of the pump. The laser pulse is focussed to a length of 1 cm and width of 100 μm.

A. Pulse wavelength

Figure 6 shows the behavior of gadolinium (Z=64) under pumping by pulses of relatively long duration 290 ps for different wavelength combinations. It can be seen that the behavior of the harmonic and mixed harmonic and fundamental pulses are very similar, as predicted due to the strong thermal conduction. The fundamental pulse alone on the other hand shows a marked difference, although again the behavior is in accord with our expectations. The electron temperature in the latter case is higher, and the peak absorption density (not shown) lower. The profile of the ionization with energy shows a much weaker variation for the fundamental than the harmonic. This is due to the density variation in the time to ionization shown in Fig. 2. Gadolinium is in fact an important transition case where the ionization time plays a critical role in determining the appropriate wavelength. For all ions of higher atomic number it is more efficient to use either harmonic or (better) a mixture of harmonic and fundamental.

We note from Table III that the density associated with the self-regulating model clearly lies well below the critical density. A useful check on the nature of the absorption process can be obtained by calculating from simulation the average single pass absorption due inverse bremsstrahlung, α, which is related to the overall absorption fraction, β, by

$$\alpha = 1 - \sqrt{\left[\frac{(1-\beta)}{R}\right]} \tag{15}$$

where R (=0.7) is the reflectivity of the critical surface. The total fractional absorption by inverse bremsstrahlung, including that in the reflected beam, is therefore $\alpha+\alpha(1-\alpha)R$. For the fundamental we obtain from our simulation, β=0.74 and α=0.39, and hence the total fractional absorption due to inverse bremsstrahlung is 0.56, whereas that at the critical surface is only 0.18.

In the case of the harmonic, the overall absorption is β =0.95, and the fractional absorption in a single pass due to inverse bremsstrahlung is α=0.74, and the total absorption by this mechanism is 0.82. Absorption is almost entirely within the plasma body. The behavior at this wavelength is thus also due to subcritical inverse bremsstrahlung with strong thermal conduction.

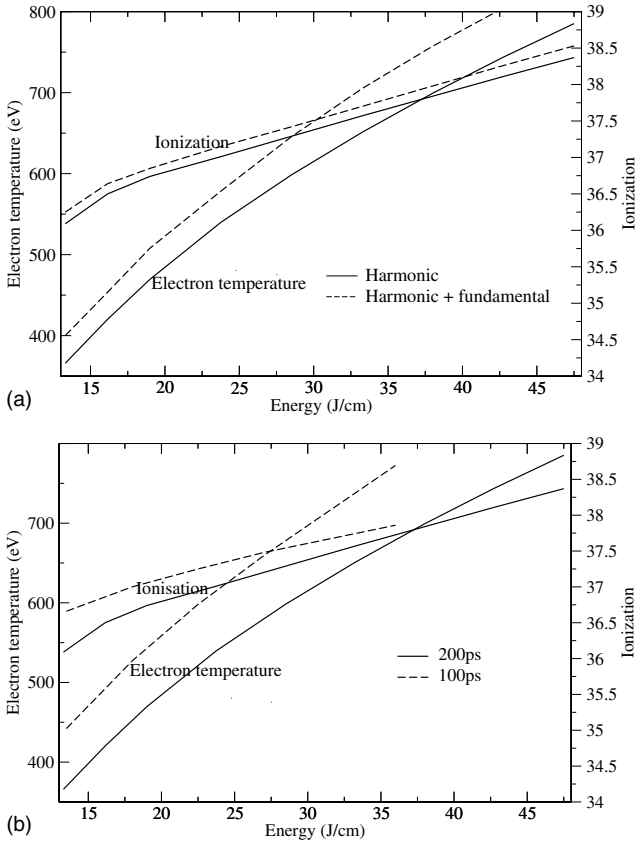

FIG. 7. Plots of ionization and electron temperature from irradiation of dysprosium by (a) a pre-pulse of 200 ps duration as function of the pump laser energy for pure harmonic and 50% admixture of harmonic and fundamental, and (b) for pulses of length 100 and 200 ps at the harmonic only.

B. Pulse length

Results from detailed simulation of dysprosium are shown in Fig. 7 which show behavior very similar to that predicted from our models for the harmonic alone, and very similar to the harmonic for the admixture of fundamental and harmonic. Assuming that we can generate laser action at the copperlike ionization stage (one less than nickel-like) we find from Fig. 7(a) that for a fundamental/harmonic pulse of 200 ps we require about 24 J/cm for dysprosium.

In Fig. 7(b) we examine the effect of changing the pulse length but maintaining constant energy. We observe that the shorter pulse is significantly hotter and that the ionization is slightly increased as a result. The plasma mass (not shown) and the spatial extent are slightly decreased. These results are consistent with the increased irradiance associated with the short pulse. The improved ionization is therefore to be balanced against a possible worsened refraction limitation. We defer until later the resolution of this problem.

The results obtained with dysprosium are basically similar using either the harmonic or the harmonic-fundamental combination. At a pulse length of 200 ps, the irradiance required with the harmonic to reach the copperlike ionization stage is clearly determined by the self-regulating picture with a strong contribution from thermal conduction. This is confirmed by the calculated single pass absorption of $\alpha=0.68$ giving a total fractional absorption due to inverse bremsstrahlung of 0.74. The electron density associated with the self-regulating model is 8.2×10^{20} cm^{-3} compared to a critical density of 4×10^{21} cm^{-3}. This behavior, namely absorption by inverse bremsstrahlung with strong upstream thermal conduction, explains the close similarity between the harmonic and mixed fundamental and harmonic cases. However, we note that there is significantly improved ionization from the mixed pulse.

C. High atomic number

At atomic number 70 (ytterbium), the minimum ionization temperature required to achieve the minimum necessary copperlike stage is estimated to be about 700 eV (Fig. 1). At 0.53 μm wavelength, the corresponding irradiances are estimated to be 4.2×10^{13} W cm^{-2} from the deflagration model and 1.8×10^{13} W cm^{-2} from the self-regulating for a pulse length of 200 ps, and 5.5×10^{13} W cm^{-2} and 3.8×10^{13} W cm^{-2} for a pulse of 100 ps. In Fig. 8 we examine the results from simulation by pulses of 100 ps duration and 50%:50% combination of harmonic and fundamental over the irradiance range 2.3×10^{13} W cm^{-2} to 8.3×10^{13} W cm^{-2}. It can be seen that only at the highest input energy was the copperlike ion produced, and that the required temperature was about 1500 eV. These values are very different from those predicted by steady state models and reflect the finite ionization time for these atomic numbers (Fig. 2).

Experimenting with a range of different pulse characteristics, varying the pulse length, the fraction of fundamental and harmonic and introducing a delay between the two does not markedly change this result, although the required temperature is reduced to less than 1 keV for pulses longer than 300 ps (Table IV). The total energy needed remains approximately the same. Due to the reduced absorption, the irradiances needed are correspondingly larger than the estimated values namely about 4.4×10^{13} W cm^{-2} for a 100 ps pulse and 3.8×10^{13} W cm^{-2} for a 200 ps. The second difficulty is seen in Fig. 8(b), where it can be seen that as the pump energy is increased the absorption by inverse bremsstrahlung decreases. This is a consequence of the higher temperatures. Lengthening the pulse, thereby increasing the plasma length and lowering the temperature restores the absorption to reasonable values.

It is clear from the above results that the longer pulse, which is better absorbed, is balanced by the greater mass of plasma produced. As a result the temperature is lower but the longer time available for the ionization to take place allows the system to reach the same condition. However, comparison with the temperatures generated in the simulation with those from the equilibrium state shows that the plasma has not yet reached the ionization steady state after a pulse of 400 ps. This is in marked contrast to the ions of lower atomic number.

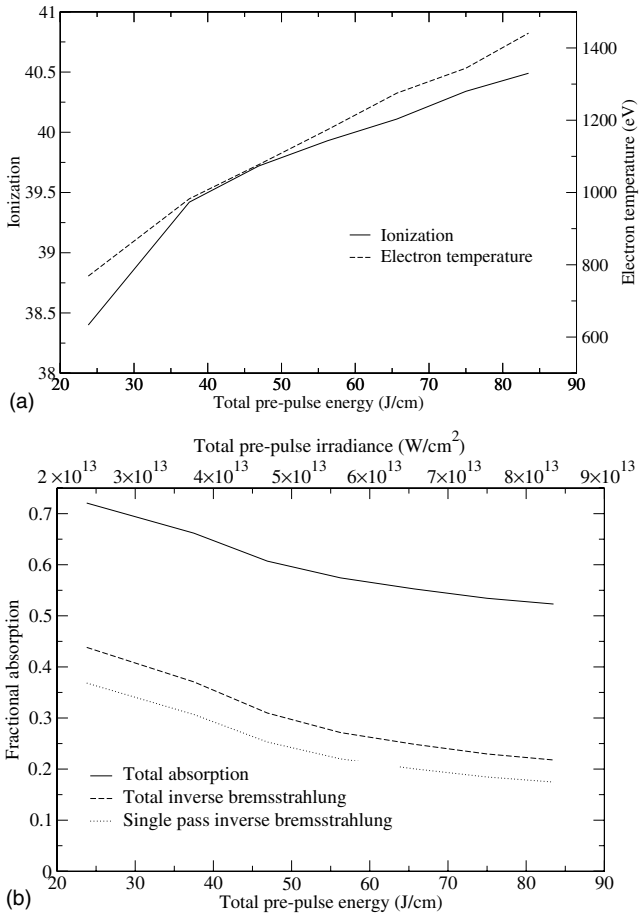

FIG. 8. Ablation characteristics by irradiation of ytterbium by a 100 ps pre-pulse of 50% admixture of harmonic and fundamental.

It is also clear from that there is no further improvement beyond a pulse length 200 ps. Further increases in pulse duration lead to increased mass and cooler plasmas without further improvement in the absorption. We therefore conclude that more than approximately 100 J/cm in the pulse of 100 μm focal spot width is needed to reach the copperlike ionization stage in ions with atomic number greater than 70. This will place severe constraints on the pumping system, unless a narrow focal spot is used.

X. GAIN GENERATION

The gain is generated by pumping through electron collisions on the appropriate transitions. Figure 3 shows that for dysprosium effective pumping can be obtained for temperatures of the order of 1 keV and that weak pumping is obtained at the ionization temperature of about 500 eV. It is therefore necessary to further heat the plasma body to generate strong gain. With the lower atomic elements such as silver, thermal conduction is not strong, and the heating can be localized in a region where the refraction effects are weak. At the higher temperatures and densities required by

TABLE IV. Conditions necessary to achieve Ni-like ionization in ytterbium under different pulse conditions.

Wavelength μm	Energy J/cm	Duration ps	Temperature eV	Fractional Absorption	Inverse Bremsstrahlung
0.53	94.0	100	1440	0.68	0.48
0.53	97.0	200	1050	0.90	0.78
0.53	53.0	100	1441	0.52	0.28
1.06	53.0	100			
0.53	46.5	200	1250	0.82	0.66
1.06	46.5	200			
0.53	46.5	300	960	0.88	0.75
1.06	46.5	300			
0.53	46.5	400	870	0.90	0.79
1.06	46.5	400			
0.53	22.5	100	1424	0.77	0.59
1.06	67.5	100 after 80 ps delay			

high atomic number elements, energy even if rapidly deposited by a short (ps) duration pulse is disseminated over the plasma body. Gain however, will be more limited in its distribution to higher density due to the ion density dependence of the appropriate coefficient. Nonetheless the general principle of localized heating still applies. Since the density profile of the plasma following pre-pulse ionization by a harmonic+fundamental combination corresponds to short wavelength heating with a steep density front at about 4×10^{21} cm^{-3} we can use the fundamental at normal incidence rather than non-normally incident harmonic for the main pulse heating. Furthermore since the plasma is already hot and the radiation absorbed locally, the main pulse can be relatively weak, typically 1/3 of the pre-pulse in energy, although short in duration, e.g. 2 ps.

A. Gadolinium

In Fig. 9(a) we show the gain which can be generated by using the harmonic+fundamental combination for the pre-pulse and the fundamental at normal incidence for the main pulse. The gain has a lifetime of about 7.5 ps in the region of low refractive index gradient before thermal conduction cools the deposition zone and the gain moves to higher density due to the gain scaling, although at a lower temperature. Figure 9(b) shows the estimated output signal after ray tracing yielding a pulse of about 7.5 ps duration limited by the gain moving to regions of strong refraction. The total output energy over a width $\sim$100 μm is about 65 μJ.

B. Dysprosium

Dysprosium shows a very similar behavior to gadolinium. The gain is relatively short lived decaying after about 15 ps as the plasma cools by thermal conduction, remaining throughout its life within a region of relatively shallow density gradient.

Figure 10 compares the output produced by different combinations of pulse length and wavelength from a 1 cm plasma column. It is clear that the strongest output is produced by the 100 ps harmonic pre-pulse which generates about 60 μJ across a 100 μm spot. The 200 ps pulse produces a significantly lower energy pulse ($\sim$20 μJ) with a

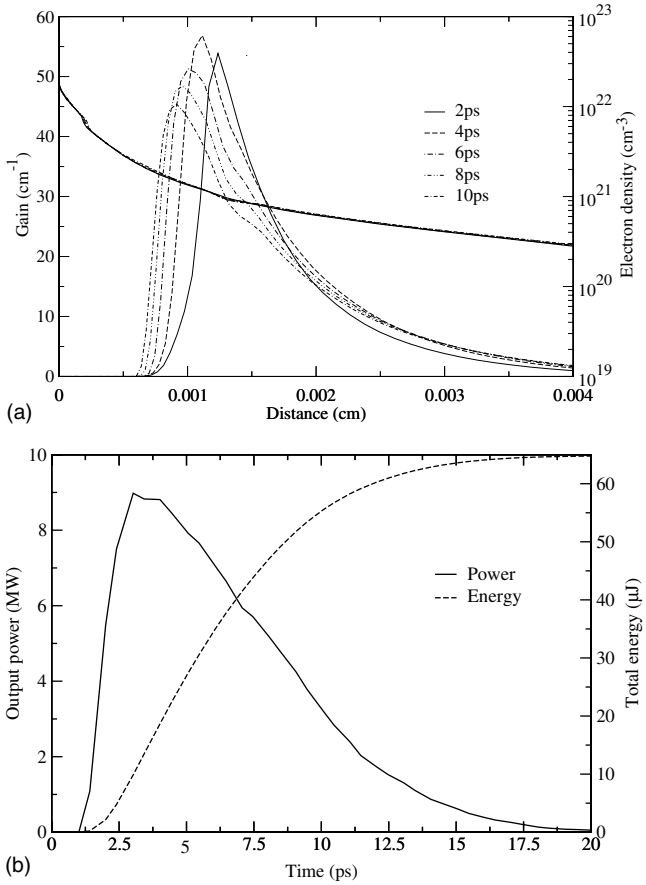

FIG. 9. Plots of gain at 64 Å and electron density (a), and output power and energy (b) for gadolinium pumped by a pre-pulse of 21 J/cm of mixed harmonic+fundamental wavelengths in 290 ps and a fundamental main pulse 7 J/cm in 2 ps at normal incidence.

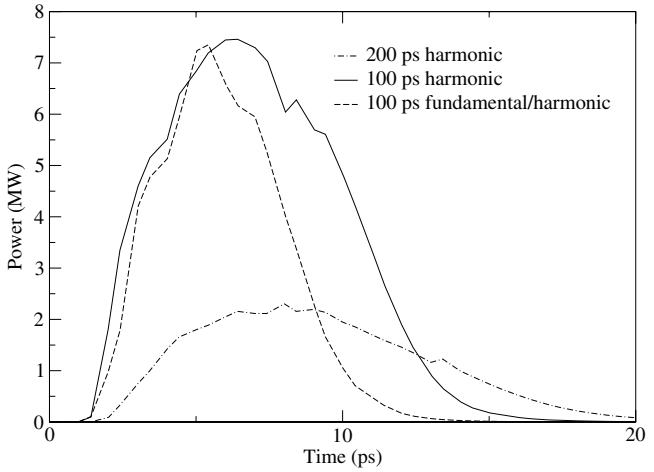

FIG. 10. Plots of the output power from a 1 cm length of dysprosium at 59 Å pumped by different pre-pulse combinations of 200 ps harmonic only, 100 ps harmonic and harmonic +fundamental wavelengths, all of 22 J/cm with the same fundamental main pulse of 5.4 J/cm in 2 ps.

longer duration, although Fig. 11 suggests that the total energy can be increased in this case by enhancing the main pulse. The differences in pulse duration and power reflect relatively small changes in the spatial profile of the refractive index, as well as gain. Figure 11 compares the output from this case with that generated by a more strongly pumped case. As may be expected the latter produces substantially more output at about 200 μJ in a pulse of about 10 ps with roughly the same temporal profile, However, the relatively small growth in the main pulse energy from 5.4 J/cm to 8.8 J/cm has generated a factor of 10 increase.

C. Ytterbium

Ytterbium as we have seen presents a different problem to the longer wavelength systems discussed earlier. In this case

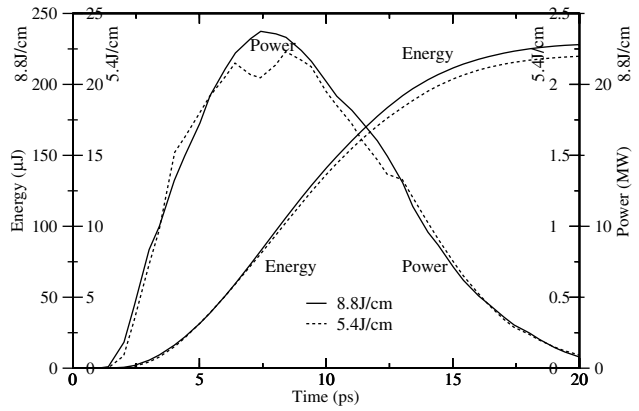

FIG. 11. Plots of the output and energy in dysprosium at 59 Å generated by pre-pulse irradiation with a pure harmonic beam of 23.75 J/cm in 200 ps and main pulse irradiation by normally incident fundamental beams of 5.4 J/cm and 8.8 J/cm. Note that in the 5.4 J/cm case both the power and energy are reduced by a factor of 10. The plasma length was 1 cm.

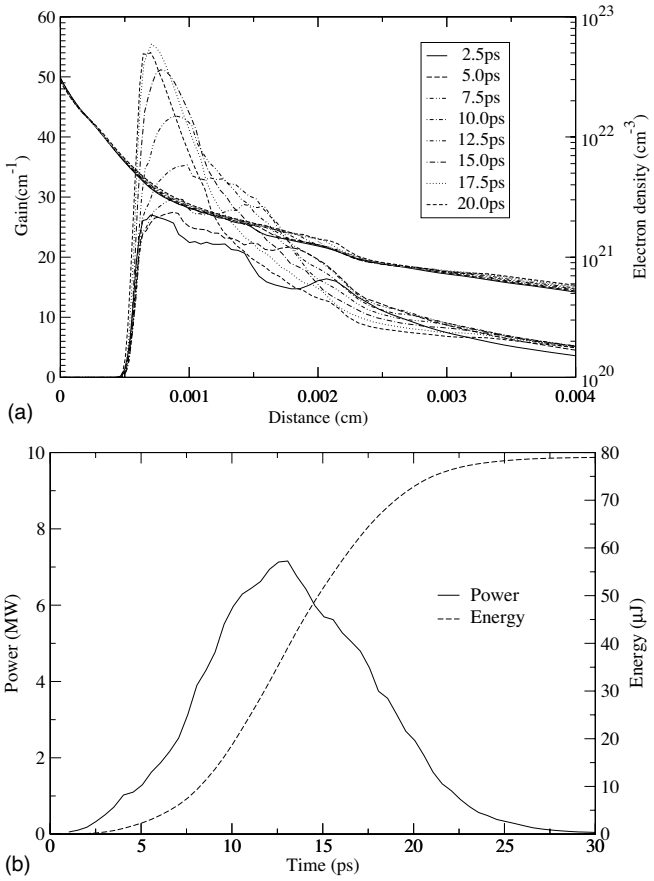

FIG. 12. Plots of the gain and electron density (a), and output power and energy (b) for ytterbium at 50 Å pumped by a combination harmonic/fundamental pre-pulse of total energy 97 J/cm in 200 ps with a fundamental main pulse of 23 J/cm in 2 ps. The plasma length was 1 cm.

the limiting condition is one of generating the ionization, which fixes the pre-pulse conditions. The main pulse is required to obtain sufficient heating against the rapid heat loss from the gain zone due to thermal conduction. Figure 12(a) shows the profiles of gain from a mixed harmonic +fundamental pre-pulse of 97 J/cm and 200 ps duration followed by a fundamental pulse of 23 J/cm in 2 ps at normal incidence. It can be seen that the density gradient is weak up to a density of about 3×10^{21} cm^{-3} and that gain of greater than about 30 cm^{-1} lasts for about 20 ps in that region. Higher gains may be generated by doubling the main pulse input energy. But a further doubling of the main pulse energy leads to a reduction in gain due to overionization. The gain has a long lifetime of about 25 ps at reasonable values ($\gtrsim$10 cm^{-1}) within the effective density region despite the fact that the plasma is becoming overionized by that time, and in fact eventually terminates it. This can be clearly seen in the plot of the power and energy output over 1 cm [Fig. 12(b)]. The total energy generated is about 80 μJ in a pulse of about 10 ps half-height.

Doubling the main pulse energy increases the gain and the output. The lifetime, however, remains approximately the same, as overionization is compensated by increased pumping rates.

XI. DISCUSSION

The principal difficulty in attempting to reduce the wavelength of collisionally pumped Ni-like soft x-ray lasers is found to be due to the temperature required to achieve the necessary ionization. In this paper we have used a relatively simple strategy to separate the ionization and pumping phases of the laser. This employs a relatively long pulse to both generate the ionization and simultaneously develop a slowly decreasing electron density profile to reduce refraction. The pumping is induced by a short high irradiance heating pulse. Clearly other strategies are possible. For example we could use a third low energy pulse to initiate plasma development to be followed by the ionization pulse. However, at the wavelengths of interest in this work (<70 Å) refraction is less of a problem than at longer wavelength, so that the density distribution is less important.

Due to the rapid increase in absorbed energy required to induce the ionization as the atomic number is increased, these plasmas start to weakly absorb laser energy due to the high temperatures. In order to avoid nonthermal electron distributions with concomitant effective energy loss it is advisable to maintain absorption by inverse bremsstrahlung. To this end the use of a shorter wavelength first (pre-)pulse is advisable. This allows us to pump the laser with the second beam at a correspondingly high density without penetrating into the region of strong density gradient, and more closely match the optimum pumping density at which the gain is maximized. In the course of these investigations we have found that a combination of the fundamental and harmonic of the Nd-glass laser at 1.06 μm wavelength for the prepulse and the fundamental alone for the main is very suitable. The strong thermal conduction in these plasmas enables the heat deposited by the fundamental component of the pulse to rapidly diffuse to higher energy, and effectively strengthen the harmonic. The use of both fundamental and harmonic, in principle, allows a more efficient use of the primary laser beam. The waste flux from the harmonic generation is available to provide the fundamental, provided any optical focusing problems can be resolved. In contrast to the longer wavelength x-ray lasers there is no benefit from introducing the main pulse at non-normal incidence.

We have used relatively simple analytic models to examine the development of plasma at the required ionization by the pre-pulse. Despite their limitations with respect to the nature of the absorption, heat conduction and ionization in these dense plasma, they have been reasonably accurate when compared with detailed simulation within the accuracy expected for such simple representations (Table III). Although not suitable for accurate estimates, the models help to identify the basic physics and scalings dominating the prepulse phase. They show that the high temperature in the plasma leads to large increases in the thermal conductivity, and as a result strong thermal conduction starts to dominate the plasma development. To some extent this is an advantage in that the plasma becomes nearly isothermal. It also gives rise to a heat front propagating into the solid and a corresponding energy loss. More damagingly it also leads to a substantial increase in the plasma mass, and therefore the net energy required. Our models show that typically the upstream hot plasma mass is greater than the downstream expanding corona. However, since the absorption is dominantly by inverse bremsstrahlung and therefore subcritical, the thermal conduction zone provides a region of relatively low refractive index gradient at a density above that due to absorption. In this region gain can develop at higher density and therefore to larger values in an acceptable refractive index profile.

The ionization pulse is the dominant one in these scenarios. The second heating pulse is a short burst of energy which rapidly heats the plasma locally and induces a rapid excitation of the relevant levels in lasing ion. Since this pulse is short, it quickly heats a smaller mass of plasma without the temperature loss needed to generate further ionization, and is therefore significantly less energetic than the prepulse. In these simulations we have found that about only about 1/3 of the energy of the first pulse is needed. Its duration must be sufficiently short that it has finished before further ionization, thermal losses or hydrodynamic effects play a role. We have found that 2 ps is satisfactory, and the length could probably be slightly increased without adverse effect—it is not a critical parameter provided the plasma is in an appropriate ionization state before onset. The output is strongly dependent on the magnitude of this pulse up to a limit determined by the fall-off of excitation rates at high temperature and saturation. If the pulse has too much energy, the gain is long lived, moving to higher density, as the plasma cools through thermal conduction and ionization. However, overionization plays a role and cuts the gain off.

We have not used GRIP pumping in this work. Since the optimum density is high, we require the gain to develop at as high a density as possible, consistent with a reasonably flat density profile. In principle we might use the harmonic as the main pulse introduced at (say) 45° to pump at (nominal) density 2×10^{21} cm^{-3}. However, in tests, we found no benefit from this approach, and discarded it in favor of normal incidence fundamental pumping, thus also avoiding the technical difficulty of frequency doubling the CPA pulse.

Ytterbium appears to form a limit to these designs. In contrast to gadolinium and dysprosium, the laser energy needed to obtain the necessary ionization is very much larger than in the other elements. This is due to the longer time needed to generate the Ni-like ion at temperatures near to the ionization temperature, to the larger conduction zone, and to the reduction in the absorption in the hot plasma. As Table IV shows any compromise between an increased temperature or longer pulse for ionization does not lead to a reduction in the required energy.

An alternative strategy, which can be proposed, is to use a relatively weak pre-pulse and a stronger main pulse than advocated thus far. In this case the plasma is initially ionized to a stage some way from the Ni-like. The heating induced by a stronger main pulse is then used both to complete the ionization and provide the excitation. Although this strategy is satisfactory at longer (>100 Å) wavelengths, it is not appropriate here. The strong thermal conduction induced by the high temperature and the relatively slow rate of ionization means that much of the energy is dissipated before gain can be established. Trial simulations confirmed this behavior and did not generate strong gains.

These results may seem disappointing. However, they are consistent with the limited experimental data available at these wavelengths. All laser action at sub-70 Å wavelengths has been generated at large facilities with high energy pulses. This work by splitting the ionization and excitation phases shows that these demands have been determined by the large energy requirements of ionization, which cannot be averted.

In all our calculations we have considered a wide body of plasma (100 μm). In practice to reduce the input laser energy one would probably use a narrow input beam. Our calculations have been made on the assumption of 1 dimensional plasma flow. Since the scale of the plasma is typically about 20 μm, we require a focal spot greater than this width. We have assumed that the pre-pulse has constant power; experimental laser systems will have a more complex temporal and spatial profiles, which will cause the estimates given here of the required irradiance to be underestimates in an experiment.

ACKNOWLEDGMENTS

It is a pleasure to acknowledge useful conversations with G. J. Tallents, J. Dunn, and T. Kuell. This work could not have been carried out without the availability of the atomic data code obtained from R. D. Cowan at Los Alamos—many thanks. This work in its early stages was supported by EPSRC and AWE.

APPENDIX A: EHYBRID

The principal code is EHYBRID, which is used to calculate the dynamics of the pump laser/plasma interaction. It consists of a $1\frac{1}{2}d$ hydrodynamic model [27,28] in which the hydrodynamic flow is treated by the one dimensional von-Neumann-Richtmyer algorithm in the direction of the normal to the target surface and by a modified self-similar expansion tangential to the surface. The initial plasma width is determined by a preset value usually taken as the FWHM of the pumping laser pulse, and is assumed to be cutoff at the plasma edge. The transition of the transverse flow from the initial quasirectangular profile to a Gaussian is accomplished by an empirical fit to a classical rarefaction propagating toward the center from the outer edge at a rate determined by the growth of the Gaussian $1/e$ profile width. Laser absorption occurs within the geometrical cross section of the plasma only, and is due to inverse bremsstrahlung. For radiation normal to the target, a preset dump at the critical density (representing resonance and nonlinear absorption) is introduced. The laser beam may alternatively be introduced at an arbitrary angle to the target normal and refracted through the plasma, in which case resonant absorption is directly included using the standard linear form. The code considers a two temperature fluid with ion and electron (flux limited) thermal conduction and ion/electron equilibration. The values of the parameters used for this work were $f=0.1$ for the flux limiting coefficient and $R=0.7$ for the critical surface reflectivity. In earlier studies modelling experiments we found that the code consistently overestimated the total energy within the plasma, due it is thought to a number of nonlinear factors which are not included in the model. To accommodate this discrepancy, we introduced an empirical absorption factor, F [14]. In this work we have not included this factor and F is set to unity throughout, although as noted earlier the fill factor is included explicitly.

Ionization and population dynamics are treated self-consistently with the hydrodynamics using an overall electron energy balance, by methods reported in earlier work [29,30]. Ionization is calculated either by using simple modified forms of the ionization/recombination rates developed by Griem [31], or by a time dependent collisional-radiative model based on either screened hydrogenic levels [26], or a detailed set of accurately calculated atomic levels. In these calculations for Ni-like ions we have used the modified Griem's model (MGM) for the stages I-$(Z-\mathrm{XXXIII})$ and $(Z-\mathrm{XXIII})-(Z+\mathrm{I})$, the screened hydrogenic system with three hydrogenic levels for stage $(Z-\mathrm{XXXII})$, with four for $(Z-\mathrm{XXXI})$, five for $(Z-\mathrm{XXX})-(Z-\mathrm{XXVIII})$, eight for $(Z-\mathrm{XXVI})$, five for $(Z-\mathrm{XXV})$, and three for $(Z-\mathrm{XXIV})$, and the full calculation for the Ni-like stage $(Z-\mathrm{XXVII})$. For the Ni-like stage the full level populations are calculated, and used to determine the laser line characteristics, spontaneous emission rate, gain, saturation irradiance, and Lorentz and Döppler linewidths.

This calculation procedure relies on a detailed set of atomic data for the lasant ion stage. In these calculations, we have used data sets for the energy levels, transition probabilities, and collision strengths for the ground state and configurations $3d^9 4s$, $3d^9 4p$, $3d^9 4d$, $3d^9 4f$, $3d^9 5s$, $3d^9 5p$, $3d^9 5d$, $3d^9 5f$, $3d^9 5g$, $3d^9 6s$, $3d^9 6p$, $3d^9 6d$, $3d^9 6f$, $3d^9 6g$, and $3d^9 6h$. These have been constructed as follows:

(i) For Ni-like gadolinium: the data set described by King *et al.* [32] extended to include hole states, a total of 274 excited levels.

(ii) For Ni-like dysprosium: data from Cowan's code [33], a total of 222 excited levels.

(iii) For Ni-like ytterbium: data from Cowan's code [33] extended to include $n=7$ levels, a total of 356 excited levels.

For some applications involving the modelling of x-ray laser plasmas, two time sweeps are carried out. The first with an unrefined mesh is used to determine the spatial extent of the active (heated) plasma region, the second uses a refined mesh in which the active region occupies 80% of the cells. This allows fine zoning of the active plasma, while retaining a block of inactive buffer material.

APPENDIX B: RAYTRACE

The second major code, RAYTRACE, uses data generated by EHYBRID to calculate the output from the laser following amplified spontaneous emission along ray paths subject to refraction. This code, which is described in Ref. [34], assumes that the laser medium is uniform along the axis of x-ray propagation to introduce a major simplification in the calculation. In the context of this work, this limits its applicability to either quiescent systems, in which the time variation is slow compared to the laser transit time, or to matched

travelling wave systems, when the x-ray beam sees a constant medium during its transit. In this latter case the output signal is obtained by a temporal integration over many ray traces. However, since these two cases are the ones of principal practical interest, the code is appropriate for most problems. If not, analytic approximations may be used to give an estimate of the expected output using averaged values obtained from the code results [12].

RAYTRACE operates by following the trajectories of a large number of spontaneously emitted rays through the plasma. Line narrowing effects, which result from the finite linewidth of the gain line, may be treated more simply as a correction instead of following the amplification of many frequency components. Since each ray is considered independently, problems arise in handling saturation, where population depletion is the result of the cumulative irradiance of a number of rays at that point. This problem is overcome by a two stage approach:

(i) In the first stage, the rays are traced independently using a geometrical ray trace through the plasma, calculating the amplification of a spontaneously emitted pulse along the ray path. At this stage, the radiation is assumed to have a rectangular (Milne) line profile, and saturation of the ray is included as a switch transition from exponential to linear amplification, which takes effect at a particular value of the gain-length along the path. This latter approximation is less severe than may at first appear. Due to the exponential nature of amplification, the dominant rays at any point in the plasma originate from the same neighborhood. Thus the saturation transition from exponential to linear growth for the dominant rays occurs at about the same gain length, which can be quite accurately estimated. At the conclusion of this stage, we have calculated quite accurately the output beam profile (width, divergence, deviation, etc.), and a series of ray averaged quantities, which can be used to correct the overall output for line profile effects and saturation. We also have upper bounds for the output of the beam within prescribed spatial and angular limits, but neglecting the effects of line narrowing and without a proper description of the saturation transition.

(ii) The second stage corrects for the omitted effects by using the analytic model [35]. This calculation is based on the model of the laser as a simple ASE medium occupying a uniform cylinder of high aspect ratio. All rays are equivalent. In practice the strongest output from experimental lasers (and from the first stage) comes from a group of narrowly divergent rays following very similar paths through the laser. Such behavior is well described by the model, provided we can identify appropriate values of the relevant parameters. The model calculates the output irradiance I_{out} as a function of the gain length on line center, $G_0\ell$, the saturation irradiance, I_s, and the "spontaneous emission irradiance," $I_0 = A_0/G_0$, where A_0 is the spontaneous emission rate per unit volume into the solid angle of the output beam and G_0 the gain on line center.

For most quantities, we take averages from the output of the first stage, weighted to reflect their importance among the rays and along their trajectories. Thus we weight the ray quantities (Y) (path length, gain length) as $\Sigma_{rays} Y E_{out}/\Sigma_{rays} E_{out}$, where E_{out} is the ray energy on output, and pointwise quantities (X) (gain, saturation irradiance and line widths) as $\Sigma_{rays}\int X dE/\Sigma_{rays}\int dE$, where E is the energy at each point on the ray. To avoid problems with the gain in regions of absorption (gain <0), the pointwise sums are only taken when $dE>0$, so that $E_{out}\approx\int dE$.

The averaged gain may be calculated in two ways either directly as a pointwise quantity or from the ray averages of gain length and path length.

The calculation of the spontaneous emission irradiance, $I_0=A_0/G_0$, presents the greatest difficulty, as the spontaneous emission rate into the beam solid angle, A_0, is not well defined by the first stage, due to the unknown solid angle. To overcome this problem, we work back from the output from the first stage, which is the solution for a Milne (square) line profile, and defines I_0, since the quantity is frequency invariant. Since the calculation E_{out} is only approximate when saturation is included, a separate value of E_{out}^{unsat} calculated without saturation is used.

$$I_0 = \frac{E_{out}^{unsat}}{\text{Area} \times [\exp(G_0\ell) - 1]}, \tag{B1}$$

where E_{out}^{unsat} is the unsaturated output within the beam solid angle, Area is the cross sectional area of the beam on exit, and $G_0\ell$ the averaged line-center small-signal gain length. We note that this quantity depends only on the (more accurate) ray averaged quantities. The spontaneous emission irradiance, thus obtained, can be used as input with the other quantities to give an accurate calculation for an arbitrary Voigt line profile, which takes into account cumulative saturation to give the output irradiance within the beam solid angle. Multiplying by the output area gives the instantaneous output power, which can be temporally integrated to give the output energy. This final result depends only weakly on pointwise averaging, which, in this result, is used only for quantities, which vary weakly within the plasma. Prior to saturation, since the output irradiance depends linearly on I_0 given by Eq. (B1), the output energy is independent of the area factor. Once saturation takes place, this linear behavior is lost, but due to the nature of saturation, the overall dependence is still weak, and the final energy is quite accurately calculated from the near field exit profile.

[1] R. Keenan, J. Dunn, P. K. Patel, D. F. Price, R. F. Smith, and V. N. Shlyaptsev, Phys. Rev. Lett. **94**, 103901 (2005).
[2] B. M. Luther, Y. Wang, M. A. Larotonda, D. Alessi, M. C. Marconi, J. J. Rocca, and V. N. Shlyaptsev, Opt. Lett. **30**, 165 (2005).
[3] J. Tümmler, K. A. Janulewicz, G. Priebe, and P. V. Nickles, Phys. Rev. E **72**, 037401 (2005).
[4] Y. Wang, M. A. Larotonda, B. M. Luther, D. Alessi, M. Berrill, V. N. Shlyaptsev, and J. J. Rocca, Phys. Rev. A **72**, 053807 (2005).
[5] G. J. Pert, Phys. Rev. A **73**, 033809 (2006).
[6] B. J. MacGowan, S. Maxon, P. L. Hagelstein, C. J. Keane, R. A. London, D. L. Matthews, M. D. Rosen, J. H. Scofield, and D. A. Whelan, Phys. Rev. Lett. **59**, 2157 (1987).
[7] B. J. MacGowan, S. Maxon, C. J. Keane, R. A. London, D. L. Matthews, and D. A. Whelan, J. Opt. Soc. Am. B **5**, 1858 (1988).
[8] B. J. MacGowan, S. Maxon, L. B. DaSilva, D. J. Fields, C. J. Keane, D. L. Matthews, A. L. Osterheld, J. H. Scofield, G. Shimkaveg, and G. F. Stone, Phys. Rev. Lett. **65**, 420 (1990).
[9] B. J. MacGowan, L. B. DaSilva, D. J. Fields, A. R. Fry, C. J. Keane, J. A. Koch, D. L. Matthews, S. Maxon, S. Mrowka, A. L. Osterheld *et al.*, in *X-ray lasers 1990 Institute of Physics Conference series*, (Institute of Physics, Bristol, 1990), Vol. 116 pp. 221–230.
[10] R. Smith, G. J. Tallents, J. Zhang, G. Eker, S. McCabe, G. J. Pert, and E. Wolfrum, Phys. Rev. A **59**, R47 (1999).
[11] T. Kawachi, A. Sasaki, M. Tanaka, M. Kishimoto, N. Hasegawa, K. Nagashima, M. Koike, H. Daido, and Y. Kato, Phys. Rev. A **69**, 033805 (2004).
[12] R. E. King, G. J. Pert, S. McCabe, A. G. MacPhee, C. L. S. Lewis, R. Keenan, R. M. N. O'Rourke, G. J. Tallents, S. J. Pestehe, F. Strati *et al.*, Phys. Rev. A **64**, 053810 (2001).
[13] H. G. Ahlstrom, Report UCRL-53106, Lawrence Livermore National Laboratory (1982).
[14] P. B. Holden, S. B. Healy, M. T. M. Lightbody, G. J. Pert, J. A. Plowes, A. B. Kingston, E. Robertson, C. L. S. Lewis, and D. Neely, J. Phys. B **27**, 341 (1994).
[15] J. Dunn, A. L. Osterheld, R. Shepherd, W. E. White, V. N. Shlyaptsev, and R. E. Stewart, Phys. Rev. Lett. **80**, 2825 (1998).
[16] R. Courant and K. O. Friedrichs, *Supersonic Flow and Shock Waves* (Interscience, New York, 1948).
[17] G. J. Pert, Plasma Phys. **16**, 1019 (1974).
[18] C. Fauquignon and F. Floux, Phys. Fluids **13**, 386 (1970).
[19] J. L. Bobin, Phys. Fluids **14**, 2341 (1971).
[20] G. J. Pert, J. Plasma Phys. **29**, 415 (1983).
[21] I. V. Afanas'ev, V. M. Krol, O. N. Krokhin, and I. V. Nemchinov, J. Appl. Math. Mech. **30**, 1218 (1966).
[22] A. Caruso, B. Bertotti, and P. Giupponi, Nuovo Cimento B **45**, 176 (1966).
[23] G. J. Pert, J. Plasma Phys. **36**, 415 (1986).
[24] G. J. Pert, J. Plasma Phys. **49**, 295 (1993).
[25] L. Spitzer, Jr., *Physics of fully ionized gases, No. 3 in Interscience Tracts on Physics and Astronomy* (Interscience, New York, 1956).
[26] R. M. More, Report UCRL-84991, Lawrence Livermore National Laboratory (1981).
[27] G. J. Pert, J. Fluid Mech. **141**, 401 (1983).
[28] G. J. Pert, Laser Part. Beams **5**, 643 (1987).
[29] G. J. Pert, J. Comput. Phys. **27**, 241 (1978).
[30] G. J. Pert, J. Comput. Phys. **39**, 251 (1981).
[31] H. R. Griem, *Plasma Spectroscopy* (McGraw-Hill, New York, 1964).
[32] R. King, G. J. Pert, K. M. Aggarwal, F. P. Keenan, and S. J. Rose, J. Phys. B **37**, 225 (2004).
[33] R. D. Cowan, *The Theory of Atomic Structure and Spectra, Los Alamos series in Basic and Applied Sciences* (University of California Press, Berkeley, 1981).
[34] J. A. Plowes, G. J. Pert, S. B. Healy, and D. T. Toft, Opt. Quantum Electron. **28**, 219 (1996).
[35] G. J. Pert, J. Opt. Soc. Am. B **11**, 1425 (1994).